Supplementary material for:

ESCRT-III CHMP2A and CHMP3 form variable helical polymers *in vitro* and act synergistically during HIV-1 budding

Grégory Effantin[1,7], Aurélien Dordor[1,7], Virginie Sandrin[2,7], Nicolas Martinelli[1], Wesley I. Sundquist[2], Guy Schoehn[1,3,4,5] and Winfried Weissenhorn[1,6]

[1]Unit of Virus Host Cell Interactions (UVHCI) UMI 3265 Université Joseph Fourier-EMBL-CNRS, 6 rue Jules Horowitz, 38042 Grenoble Cedex 9, France
[2]Department of Biochemistry, University of Utah School of Medicine, Salt Lake City, Utah 84112-5650, U.S.A.
[3]CNRS, Institut de Biologie Structurale-Jean-Pierre Ebel, UMR 5075 41, rue Jules Horowitz, 38027 Grenoble Cedex, France
[4]CEA, Institut de Biologie Structurale-Jean-Pierre Ebel, UMR 5075 41, rue Jules Horowitz, 38027 Grenoble Cedex, France
[5]UJF-Grenoble-1, Institut de Biologie Structurale-Jean-Pierre Ebel, UMR 5075 41, rue Jules Horowitz, 38027 Grenoble Cedex, France

[6]Correspondence: weissenhorn@embl.fr; Tel: +33 (0)4 76 20 72 81; Fax : +33 (0)4 76 20 94 00

[7]These authors contributed equally

Inventory of Supplementary Material:

Supplementary Figures 1 - 8

Figure S1:

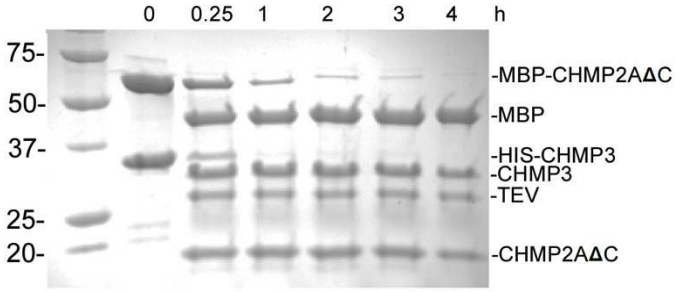

Figure S1: TEV protease removes MBP and the His tag efficiently from MBP-CHMP2AΔC-His-CHMP3 tubes. Removal of MBP from MBP-CHMP2AΔC by TEV protease was monitored over a period of 4 hours by SDS PAGE analysis. The identity of each band is labeled on the right and the molecular weight markers are indicated.

No significant differences in tube diameters were observed when tubes with completely removed MBP were compared to tubes with partially (~70%) removed MBP (data not shown).

Figure S2:

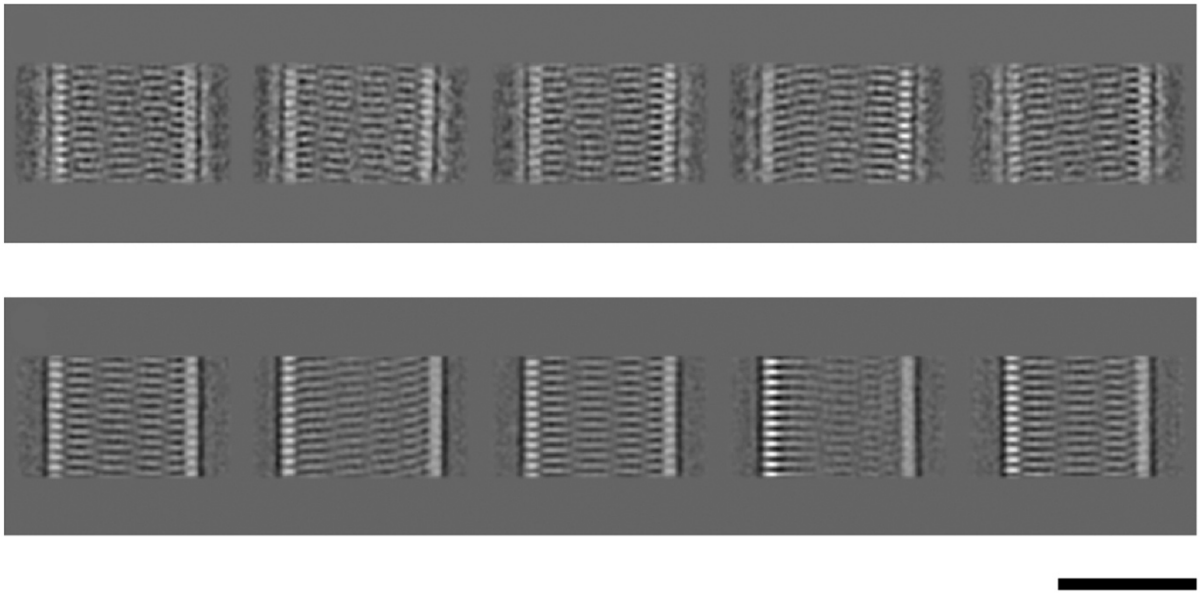

Figure S2: The presence or absence of MBP does not change the 2D class averages of CHMP2AΔC-CHMP3 tubes. Examples of five 2D class averages of CHMP2AΔC-CHMP3

tubes obtained after 2D classification of cryo-EM images of tubes with MBP attached to CHMP2AΔC (upper panel) and tubes in which MBP was removed by TEV protease cleavage (lower panel). Both tube populations (uncleaved and cleaved) derived from the same purification batch. Scale bar is 400 Å.

Figure S3:

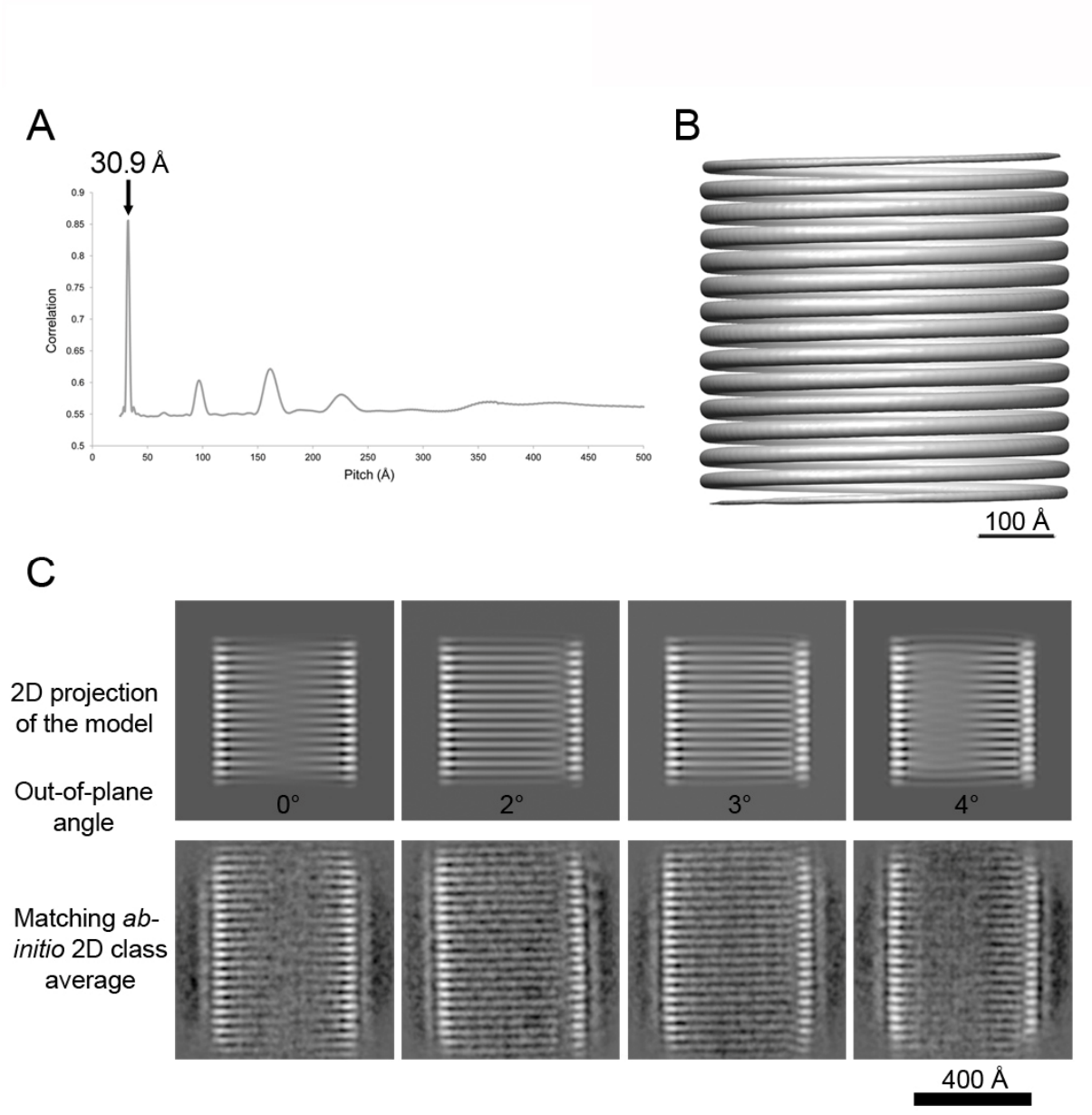

Figure S3: CHMP2A-CHMP3 tubes giving rise to the line-like pattern class average are best described by a 1-start helix with a 30.9-Å-pitch.

(A) Correlations calculated between the 2D class average (shown in Figure 2A) and the in-plane 2D projections of 3D models as a function of the pitch of the computed 3D models. The value of the pitch resulting in the highest correlation is indicated.

(B) Structural model of a helical tube with a pitch of 30.9 Å, producing a maximum correlation (as indicated in A) is shown as an isosurface in grey; the surface of the model appears smooth as an arbitrary 100 subunits per turn have been imposed.

(C) Examples of 2D projections of the 3D model shown in (B) calculated at different out-of-plane angles (indicated at the bottom of each 2D projection image). *Ab-initio* 2D class averages calculated independently from the 3D model that match well with some of the out-of-plane 2D projections are also shown to further highlight the correctness of the pitch estimated in Å.

Figure S4: CHMP2A-CHMP3 tubes giving rise to the column-like pattern class average with 5 columns are best described by a 6-start helix having a 181-Å-pitch. (A) Calculated correlations between the 2D class average (shown in Figure 2B) and the in-plane 2D projections of 3D models as a function of the pitch of the computed 3D models. The value of the pitch resulting in the highest correlation is indicated.

(B) Structural model of a helical tube with a pitch of 181.1 Å, producing a maximum correlation (as indicated in A) is shown as an isosurface in grey; the surface of the model appears smooth because an arbitrary 100 subunits per turn were imposed.

(C) Examples of 2D projections of the 3D model shown in (B) calculated at different out-of-plane angles (indicated at the bottom of each 2D projection image). *Ab-initio* 2D class averages calculated independently from the 3D model and matching well with some of its out-of-plane 2D projections are also shown to further highlight the correctness of the pitch estimated in Figure 2.

(D) Evidence of rotational symmetry of the order n (Cn) along the helical axis of the tube; 2D class averages displaying inversion symmetry (the inversion center is represented as a dot) and mirror symmetry (the mirror plane is represented as a continuous line).

Figure S4:

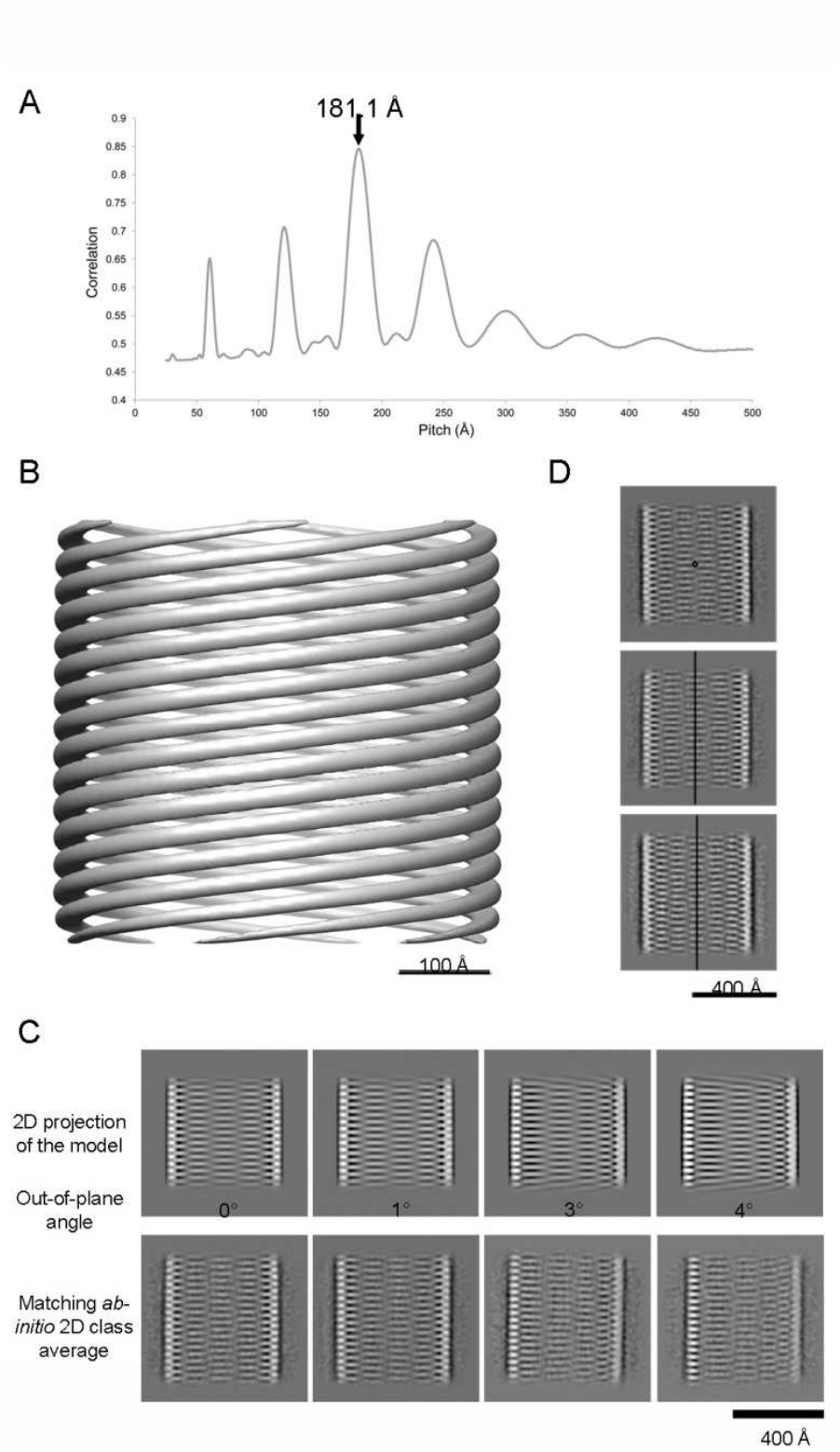
A
181.1 Å
Correlation
Pitch (Å)
B
100 Å
D
400 Å
C
2D projection of the model
Out-of-plane angle
0°
1°
3°
4°
Matching *ab-initio* 2D class average
400 Å

Figure S5: Characteristics of 3D reconstructions of CHMP2AΔC-CHMP3 tubes.

(A) Plot of the Fourier Shell Correlation (FSC) as a function of resolution (in log scale) calculated between two independent 3D reconstructions. The resolution at FSC=0.5 is 22.4 Å.

(B) In plane 2D projection of the 3D reconstruction shown in Figure 3 and its corresponding 2D Fourier transform showing a single layer line at 30 Å.

(C) Central section of the final 3D reconstruction shown in Figure 3 viewed from the top. The half image at the left shows the structure prior to imposition of helical symmetry (in IHRSR) and the right half image shows the structure after imposition of helical symmetry.

Figure S5:

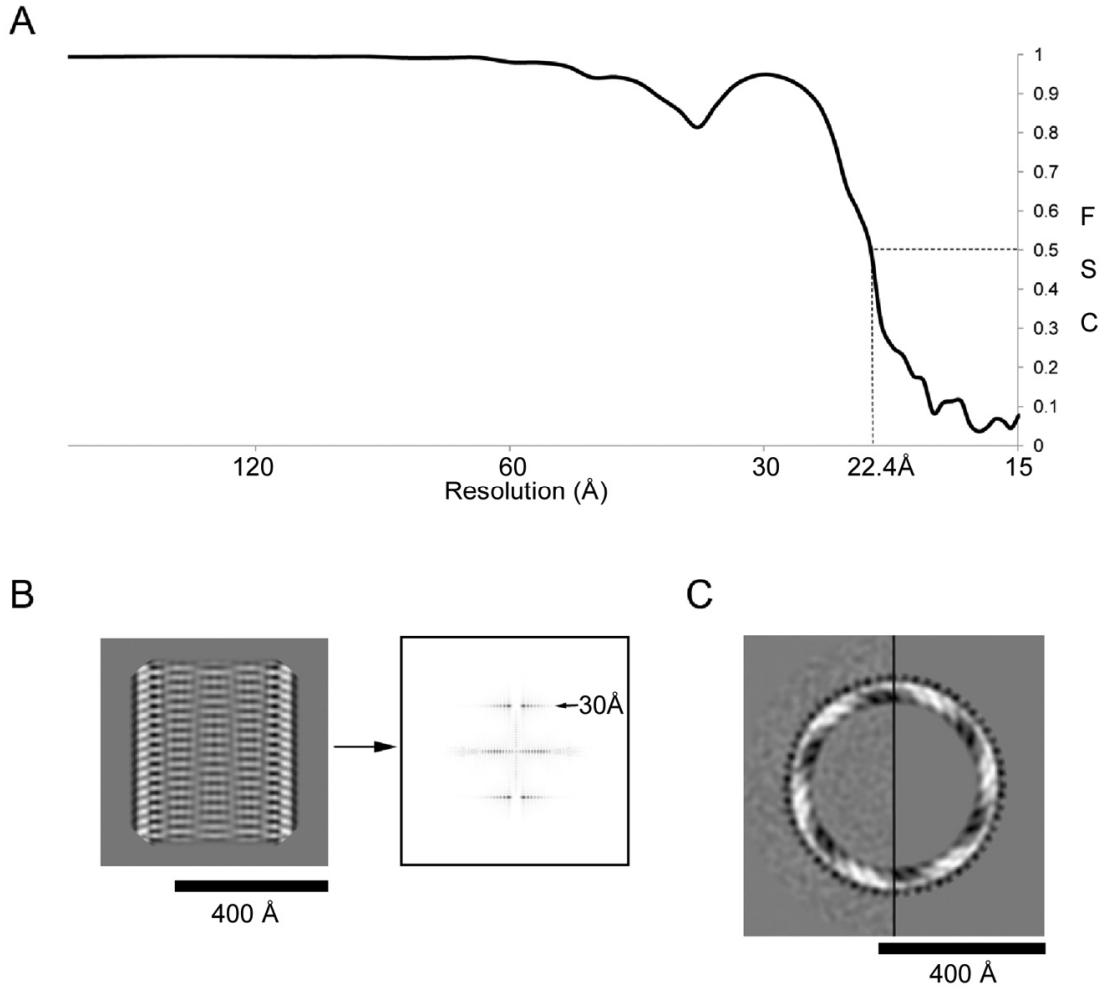

Figure S6: Comparison between cryo-EM reconstrucions of CHMP2A-CHMP3 tubes having different diameters.

(A) Isosurface representation of the 460-Å-diameter reconstruction compared to the 485-Å-diameter reconstruction (left: front view, right: same view as left but with the front half removed and 10° rotated around the X axis of the page to reveal the elongated shape of the unit cell). Two consecutive helical asymmetric units are colored differently to highlight their global similarity. Scale bar is 100 Å

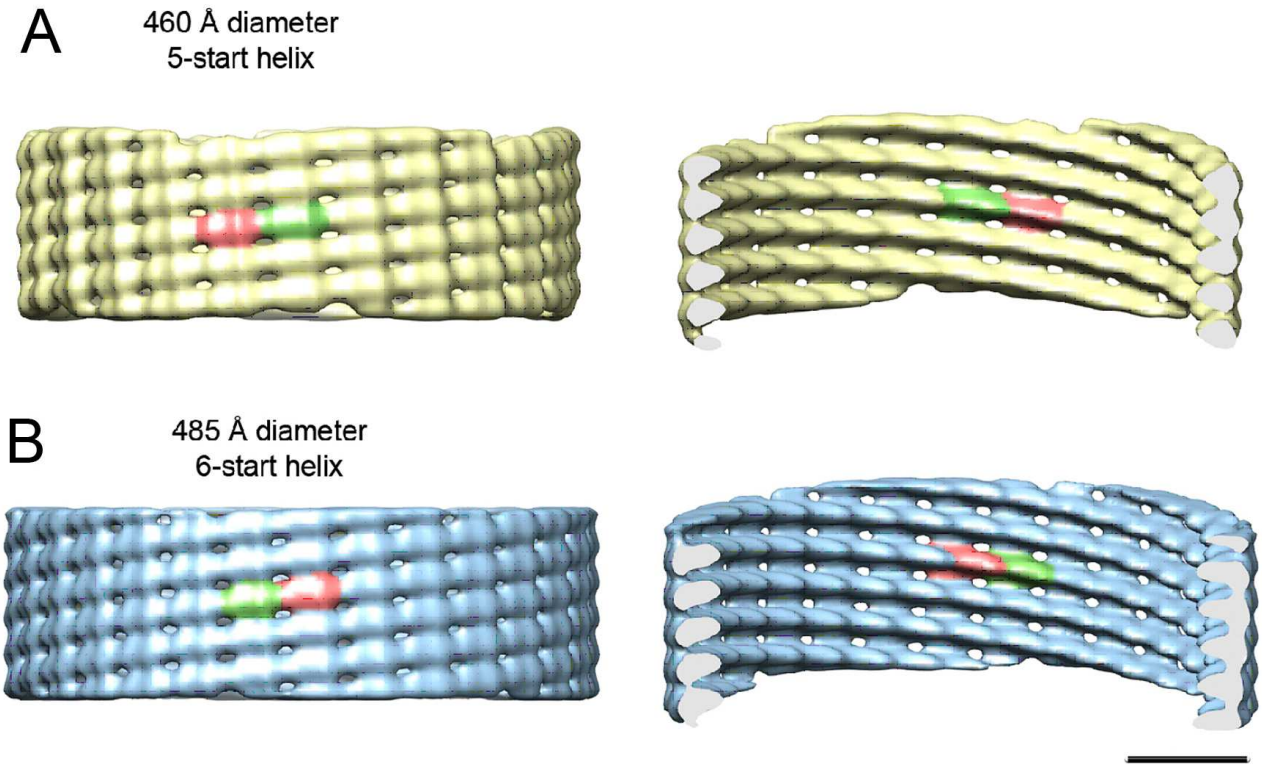

Figure S7: Comparison of CHMP3 docking into cryo-EM maps of opposite hands.
Zoomed views on 2 consecutive monomers docked inside the cryo-EM maps of inverted hands. The cryo-EM densities are shown as an isosurface in transparent gray or salmon color for the right and left-handed reconstructions respectively. Two adjacent CHMP3 monomers are shown in green and red ribbons in (A) and yellow and magenta in (B). In (A) and (B), the top panels are a front view, the middle one are the same as the top panels but viewed from the inside. The bottom panels are a top view of the two fits.

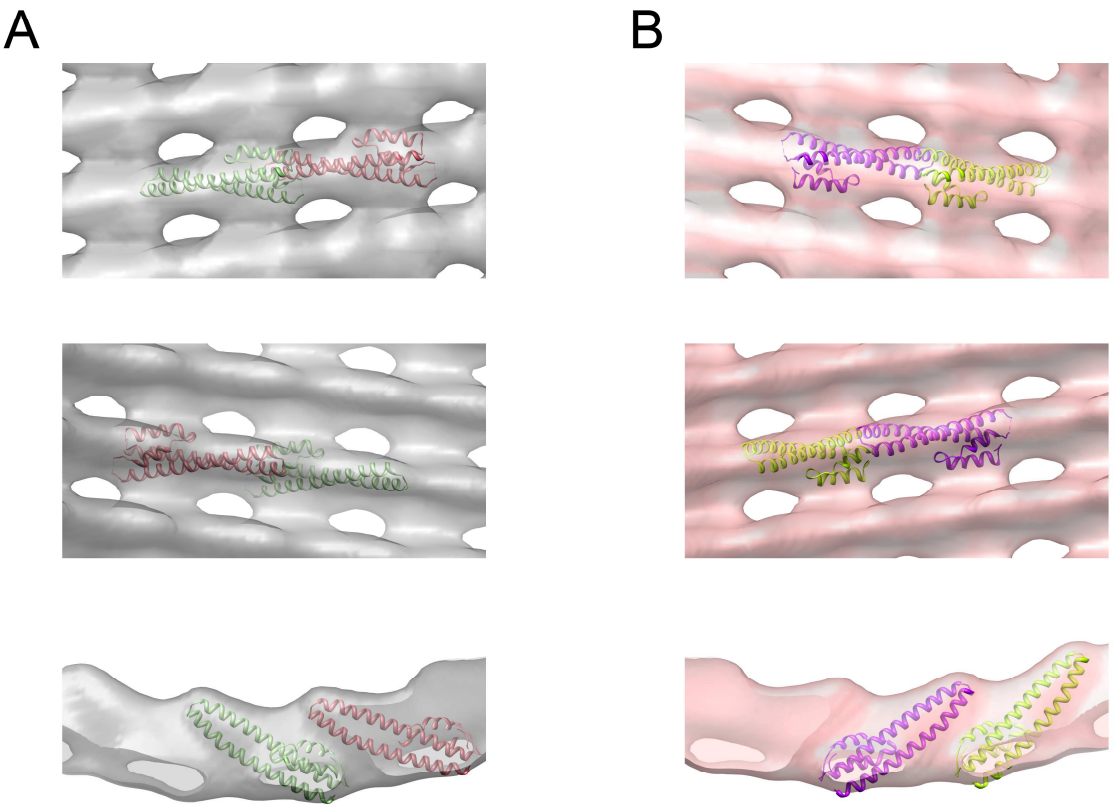

Figure S8: Biosensor analyses of binary CHMP2A, CHMP2B, CHMP3 and CHMP4B interactions.

A

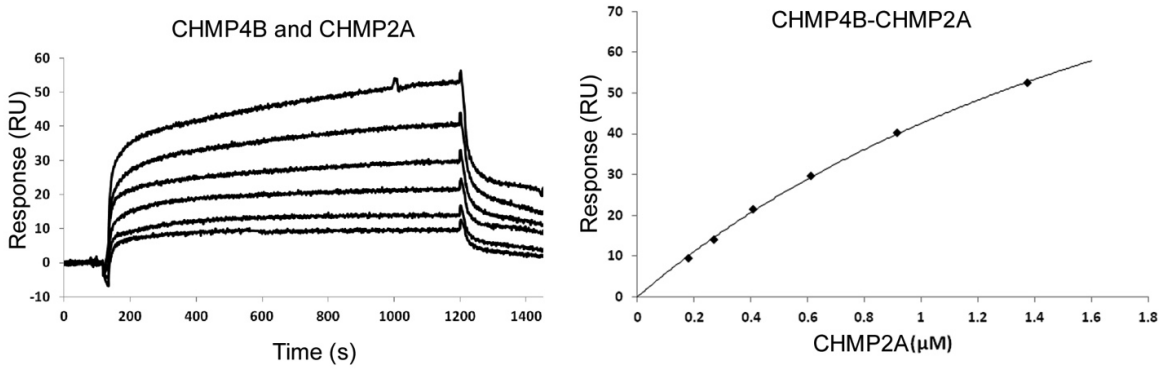

(A) Left Panel: Biosensor binding analysis of the CHMP4B-CHMP2A interaction. Sensorgrams from different MBP-CHMP2AΔC dilutions (181 nM, 271.5 nM, 407 nM, 611 nM, 916.4 nM, 1.375 µM) binding to immobilized MBP-CHMP4B$_{\Delta C\text{-}Alix}$.

Right Panel: Hyperbolic fitting of equilibrium responses from the sensograms at left resulted in a K_D of 2.43 $\pm$ 0.21 µM.

B

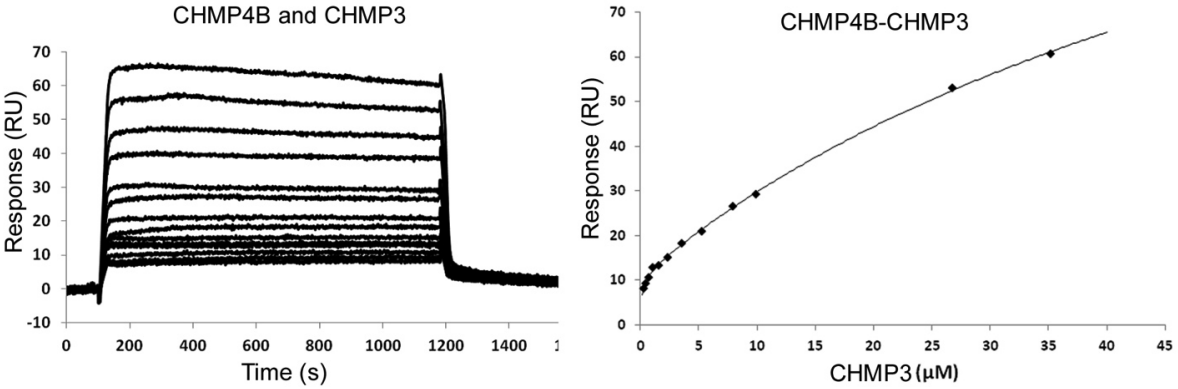

(B) Left Panel: Biosensor binding analysis of the CHMP4B-CHMP3 interaction. Sensorgrams from different CHMP3 dilutions (309 nM, 463 nM, 695 nM, 1.04 µM, 1.56 µM, 2.35 µM, 3.52 µM, 5.28 µM, 7.92 µM, 9.9 µM,11.88 µM, 17.82 µM, 26.73 µM and 35.2 µM) with immobilized MBP-CHMP4B$_{\Delta C\text{-}Alix}$..

Right Panel: Hyperbolic fitting of equilibrium responses from the sensograms at left resulted in two K_Ds, K_{D1} = 0.15 ± 0.04 µM and a lower affinity binding as evident from K_{D2} = 69 ± 12 µM, which probably reflects CHMP3 polymerization at high concentrations. Data points corresponding to 11.88 and 17.82 µM were removed as they were impacting strongly the standard error values of the dissociation constants.

C

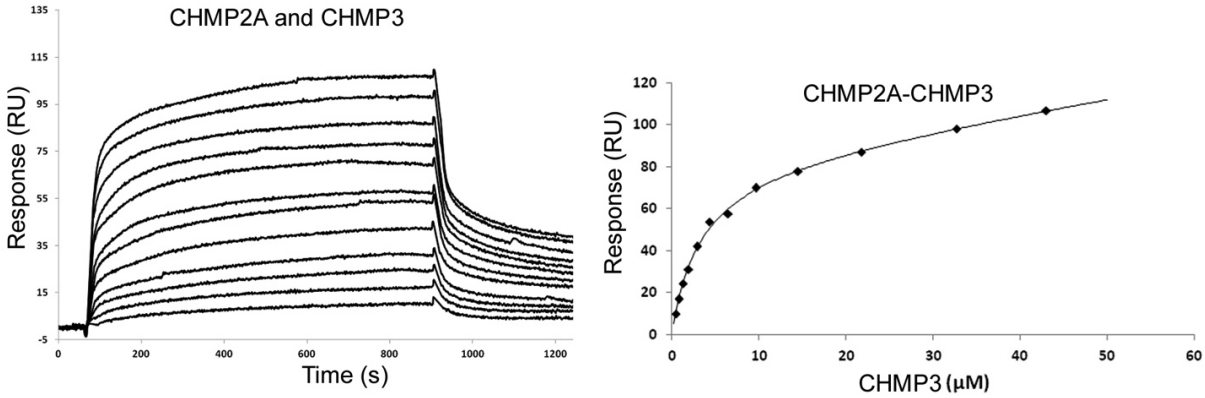

(C) Left Panel: Biosensor binding analysis of the CHMP2A-CHMP3 interaction. Sensorgrams of different CHMP3 dilutions (430 nM, 847 nM, 1.27 µM, 1.91 µM, 2.87 µM, 4.3 µM, 6.45 µM, 9.68 µM, 14.5 µM, 21.8 µM, 32.7 µM, 43 µM) binding to immobilized MBP-CHMP2AΔC.
Right Panel: Hyperbolic fitting of equilibrium responses from the sensograms at left resulted in a K_D of 3.2 ± 0.2 µM.

(D) Biosensor binding analyses of the CHMP2B-CHMP4B interaction (upper panel). The analyte CHMP2B-His_6 was injected at increasing concentrations from 0.144, 0.576, 0.72 to 0.96 µM and the globally fitted kinetic constants are listed below.
Middle panel: SPR analysis of the CHMP2B-His_6-CHMP3ΔC interaction; the analyte CHMP3ΔC was injected at concentrations of 0.0975, 0.130, 0.195, 0.390 and 0.780 µM.
Lower panel: Table listing the kinetic constants of the interactions shown in the upper panels.

D

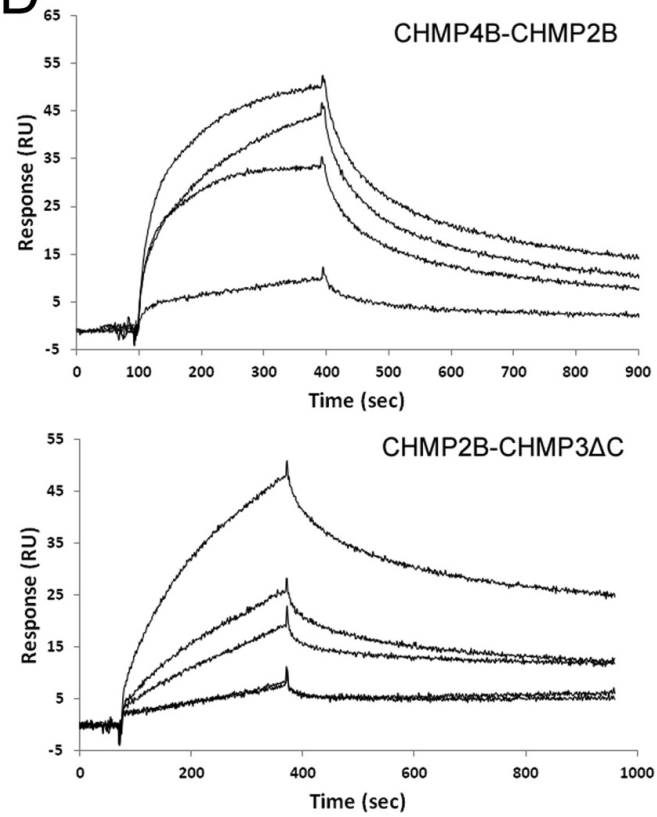

Analyte	Ligand	k_a (10^3 M^{-1} s^{-1})	k_d (10^{-3} s^{-1})	K_D (μM)	χ^2
CHMP2B	CHMP4B	6.9 ± 0.2	3.9 ± 0.05	0.56	1.43
CHMP3ΔC	CHMP2B	1.9 ± 0.07	2.6 ± 0.04	1.4	0.38